A Comparison of Force Sensing Techniques for Planetary Manipulation

Daniel Helmick, Avi Okon, and Matt DiCicco
Jet Propulsion Laboratory
4800 Oak Grove Dr.
Pasadena, CA 91109
818-354-3226
firstname.lastname@jpl.nasa.gov

Abstract—Five techniques for sensing forces with a manipulator are compared analytically and experimentally[1,2]. The techniques compared are: a six-axis wrist force/torque sensor, joint torque sensors, link strain gauges, motor current sensors, and flexibility modeling. The accuracy and repeatability of each technique is quantified and compared. The relative complexity and the impact on flight design of each technique are also compared. The results presented can be used in a trade study for missions requiring manipulator force sensing capabilities.

TABLE OF CONTENTS

1. INTRODUCTION

As more advanced tasks such as coring, drilling, grasping, scooping, constructing, and assembling need to be performed on planetary surfaces, more precise interaction with the environment becomes necessary. This drives the need to better sense the interaction forces with the environment. Better sensing also leads to lower required design margins, and thus can directly lead to lower mass and lower power designs. This paper analytically and experimentally compares five manipulator sforce sensing techniques to evaluate accuracy, repeatability, sensor breadth, and the impact on flight design of each. The techniques compared are: a six-axis wrist force/torque sensor, joint torque sensors, link strain gauges, motor current sensors, and flexibility modeling. These five techniques were chosen because they span the known trade space of force sensing in terms of complexity (the flexibility model being the simplest and the six-axis force/torque sensor being the most complex). The flexibility modeling is more of an estimation technique rather than a sensing technique, but it is important to include it in this comparison because it is the only technique that has actually been used on another planet's surface. Three of the five techniques require the use of strain gauges, which have never been used on a landed flight mission and therefore contain a certain amount of risk. An effort to qualify a low temperature strain gauge is discussed. The other two techniques, motor current sensing, and flexibility modeling, use readily available sensing, motor currents and motor positions, respectively, and are therefore much simpler to integrate into a flight system.

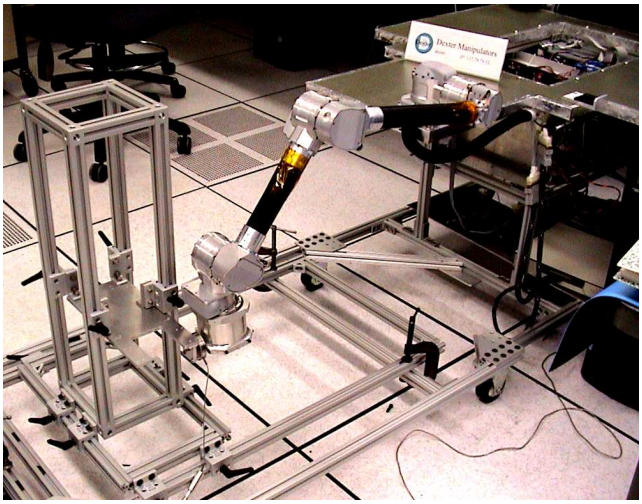

Figure 1: Five-DOF Experimental Arm with Force Sensors

Section 2 describes the setup used to perform the experiments, including the arm used to apply forces to the environment and the sensors used to measure these forces.

The experiments were performed in the Planetary Manipulation Lab at the Jet Propulsion Lab (JPL) with a five degree-of-freedom (DOF) arm (see Figure 1) that is kinematically equivalent to the Mars Exploration Rovers (MER) Instrument Deployment Device (IDD). The experimental arm is instrumented with a six-axis force/torque sensor, joint torque sensors, link strain gauges, and motor current sensors. Results from MER IDD calibration experiments [1] are used to compare the flexibility model approach.

[1] 0-7803-8870-4/05/$20.00© 2005 IEEE
[2] IEEEAC paper #1423, Version 5, Updated October 27, 2005

Section 3 discusses results obtained from analysis and the experiments described in Section 2. Quantitative results of accuracy are shown for each of the five sensor types. Repeatability is addressed for each sensing technique. The sensor breadth (a description of the information provided by the sensing technique) is discussed for each sensor type.

Section 4 discusses the impact of each sensing technique on the flight design of the manipulator. It also discusses the various levels of risk and complexity of each technique.

Section 5 summarizes the results of this study and expands on conclusions drawn throughout the paper.

2. EXPERIMENTAL SETUP

Arm Description

The arm used in these experiments is a five-DOF arm with a kinematic configuration of yaw-pitch-pitch-pitch-yaw (see Figure 1). The joints are driven by Maxon RE016 brushed motors, with a 5535:1 gear ratio (a combination of a planetary gearhead and a harmonic drive at the output) and 512 count magneto-resistant encoders. Each motor is controlled using an LM629 motor controller chip in combination with an LMD16200 H-bridge.

Sensor Descriptions

The arm is instrumented with a six-axis wrist force/torque sensor that measures the wrench (three forces and three torques) at the end-effector, custom designed joint torque sensors with redundant strain gauge bridges that measure the output torque of each of the joints, link strain gauges on the two links of the manipulator that measure bending and twist strains for each of the links, and motor current sensors that measure the motor current of each of the five motors of the arm. The experimental setup for the flexible kinematics can be found in [1].

Six-axis Force/Torque Sensor — Attached to the last joint is an ATI Mini-45 SI-145-5 six-axis force/torque sensor. This is a commercial-off-the-shelf (COTS) sensor which is comprised of six silicon strain gauges arranged in a fashion to resolve the wrench at the point of contact when multiplied by the provided calibration matrix.

Joint Torque Sensors – Four custom joint torque sensors are attached to the output of each of the first four joints of the arm. The outer part of the sensor bolts onto the output of the harmonic drive (flexspline flange) and the inner part fastens to the outer housing of the joint. Four silicon strain gauges, in a full bridge setup, are affixed to each of the two beams that connect the inner to the outer parts of the sensor. The bridge measures the bending moment of the beam caused by the torque output of the harmonic drive. Each joint sensor has a redundant output; however, only the best (determined by calibration) of the two is used for the force-sensing test.

In contrast to the six-axis force/torque sensor which resolves the actual loads in Cartesian space directly, these sensors measure the load in joint space as joint torques. The kinematic mapping from joint space to Cartesian space is represented by the manipulator Jacobian, *J*. For a given set of joint angles, the Jacobian, a $6 \times n$ matrix (where n is the number joints), is the linear transformation from a vector of joint velocities, $\dot{\vec{\theta}}$, to a vector of the Cartesian (translational and rotational) velocities, $\vec{v}$, of a specific point on the manipulator:

$$\vec{v} = J\dot{\vec{\theta}} \tag{1}$$

where $\vec{v} = \begin{bmatrix} v_x & v_y & v_z & \omega_x & \omega_y & \omega_z \end{bmatrix}^T$.

From the principle of virtual work, the transpose of the Jacobian is a linear transformation from Cartesian load, *F*, to the joint torques, $\vec{\tau}$.

$$\vec{\tau} = J^T \vec{F} \tag{2}$$

To resolve the load applied by the manipulator, the inverse of the Jacobian transpose is taken. For non-square Jacobian matrices, the force on the end-effector can be computed with the Moore-Penrose matrix pseudo-inverse. When the number of joints is less than six, as in this case, the linear system is underdetermined; thus there are infinite solutions for *F*. For this reason, an assumption is made that the torques at the point of contact are all zero. With this assumption the Jacobian transpose is a 5×3 matrix, and the linear system becomes overdetermined. Thus the pseudo-inverse solution is a least squares fit that results in the minimum residual solution.

Link Strain Gauges – The link strain gauges consist of Micron Instruments silicon strain gauges mounted on the two links of the manipulator. They are configured in two half-bridges and a full bridge that measure link bending in two directions and twist about the link's axis, respectively. The relationship between the moment load and the sensor output voltage is determined via a calibration procedure.

The relationship between the moments and the force at the end-effector are defined by:

$$M = r \times F \tag{3}$$

where *M* is the sensed moment, *r* is the vector from the contact point to the location of the sensed moment, and *F* is the force at the point of contact

The cross product operator is not invertible and thus there

are an infinite number of force solutions that results in the sensed moment. Figure 2 below illustrates this in a simple 2D case. It shows two orthogonal force components applied with unit length moment arms. The force resultant cannot be determined, because the system of equations is underdetermined.

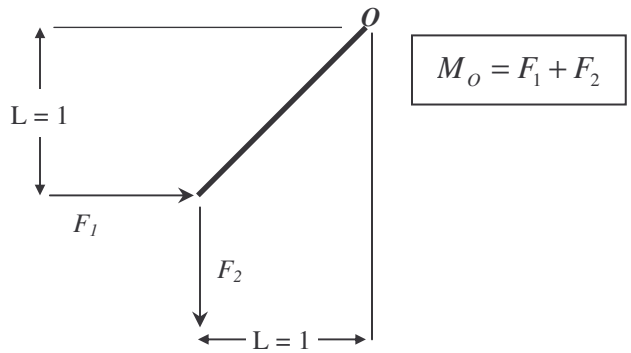

Figure 2: Underdetermined Force/Moment Equation Diagram

With two sensed moment locations, the formula becomes:

$$\begin{pmatrix} M_1 \\ M_2 \end{pmatrix} = \begin{pmatrix} r_1 \\ r_2 \end{pmatrix} F \qquad (4)$$

where

$$r_n = \begin{pmatrix} 0 & -r_z & r_y \\ r_z & 0 & -r_x \\ -r_y & r_x & 0 \end{pmatrix}, \qquad (5)$$

M_n is a 3x1 vector of measured moments for link *n*, and F is a 3x1 vector of forces at the end-effector. The problem of solving for *F* becomes overdetermined, which is then solved to find the best *F* in a least-squares sense. Again, an assumption is made that the torques at the point of contact are all zero, in order to make the problem solvable.

Motor Current Sensors – The motor current sensors consist of a resistor coupled with the current mirror on the LMD18200 H-bridge. This signal is transformed into an estimate of the joint torque using a factor based on the motor torque constant, the gear ratio, and the gear train efficiency.

Flexible Kinematics – This is more of an estimation technique than a sensing technique. It is useful to include it in this discussion for several reasons. The most important reason is that this is the technique that MER uses to apply the preload for the Rock Abrasion Tool (RAT) [1]. Another reason is that it is the simplest technique in terms of hardware complexity, because it uses only sensors that are already necessary for normal arm operations, namely, joint position sensors (motor encoders).

This technique uses a stiffness model of the arm to predict the force applied by 'overdriving.' Contact with the environment is sensed using contact switches, then the arm is driven along the estimated contact normal 'through' the contact position by a distance calculated with the flexibility model. This results in a force that is approximately the same as the input to the model.

Experimental Procedure

The sensors were tested at a number of workspace locations (see Table 2, in Appendix A) in front of and below the base frame of the arm. Without loss of generality, the experiments were performed in one vertical plane of the workspace. Because the workspace of the manipulator is defined by revolving this plane about the first joint axis these results are valid for the entire workspace of the arm.

The experiments were performed by driving the end-effector at a constant Cartesian velocity against a fixed rigid single-axis load cell sensor (a Futek L1050, with 0.9 N accuracy) (see Figure 4) in the +x, +y, and +z directions in the rover reference frame (see Figure 3) until the magnitude of the applied force (measured by the six-axis force/torque sensor) exceeded a threshold of 40 Newtons. The end-effector velocity was then reversed until the applied force was close to zero. During these moves, data from all of the sensors were collected simultaneously and logged.

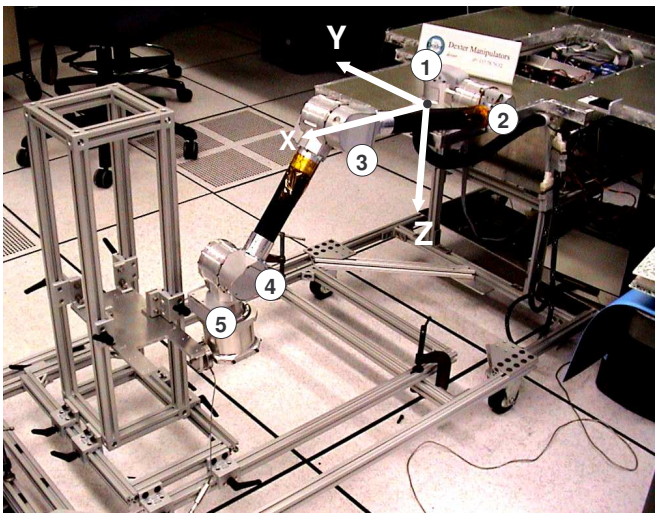

Figure 3: Arm Coordinate and Joint Number Labels

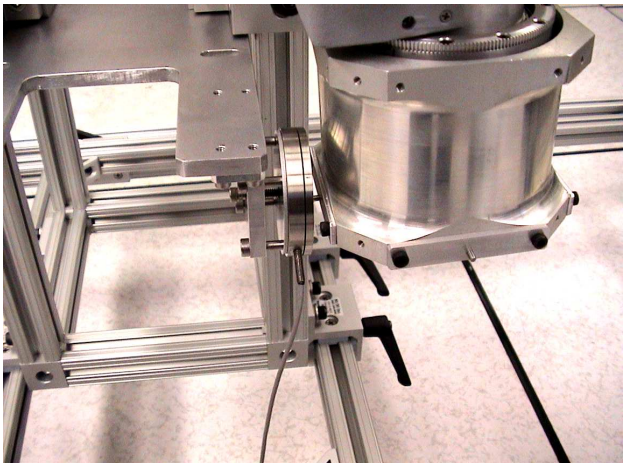

Figure 4: End-Effector in Contact with Load Cell

3. Analytical and Experimental Results

Six-axis Force/Torque Sensor

Accuracy – To determine the accuracy of this sensor, its output is compared to the single-axis load cell that the end-effector contacted during each test. Since the load cell is only sensitive to the force in one direction (it is designed to reject all other loads), only the six-axis force/torque sensor output in that direction is used to calculate the error. The readings from both sensors have been subtracted from the data of the respective sensor. This, in essence, zeroes the sensors just prior to each run.

The RMS of the error is computed for the duration of each experiment run, including both the ramping up and ramping down of the applied load. The error is the difference between the load cell reading and the output of the six-axis force/torque sensor in the load cell normal direction.

Table 1 shows the runs with the greatest and least RMS error and the standard deviation of the error over all runs.

Figure 5 shows least-square fits of the force/torque sensor values versus the load cell readings with the y-intercept fixed at zero. The best and worst cases (based on RMS error) are shown for the x, y, and z directions, respectively. A slope of one indicates that the sensor has the same reading.

If the single-axis load cell is considered truth, the six-axis force/torque sensor is accurate within its specifications, which is ±1% of the full range: 1.45 N, 0.05 Nm.

One potential source of error (slope ≠ 1) may be from the projection of the measured force from the force/torque sensor in the direction of the single-axis load cell. This misalignment may have existed in one or some combination of the following:

1. The mounting of the load cell with respect to the rover.
2. Computed pose error due to joint zero-position error.

Repeatability – The 6-axis force/torque sensor is quite invariant to the end-effector's position in the workspace. This is expected since the sensor's magnitude performance is not dependent on any aspect of the manipulator's configuration. However, the coordinate frame of the sensor is computed using the manipulator kinematics. As a result, any error associated with the pose of end-effector, thus the orientation of the force/torque sensor, can result in false measurements of the force/torque vector directions.

As with all of the techniques using strain gauges there is a potential dependency on temperature. There are common techniques to make these sensors temperature independent. An effort described in the Impact on Flight Design section will quantify the temperature dependencies of a strain gauge.

Sensor Breadth – The six-axis force/torque sensor produces three orthogonal force and moment loads at the sensor frame origin. This information can be used in two ways. If the location of the contact point is known, the sensor reading can determine the force and moment at the interface with the environment. If it is assumed that the end-effector has a zero-moment interaction with the environment (i.e. loads are forces only), the sensor reading can estimate the point of contact or the location of the reaction force resultant.

The major deficiency associated with the six-axis force torque sensor is "numbness" below the sensor mount location. A sensor mounted at the wrist cannot detect collisions between the manipulator and the environment or the rover. This deficiency is only shared with the flexible kinematics technique; all of the other sensing techniques can detect such collisions.

Joint Torque Sensors

Accuracy – The torque at each joint is determined by scaling and biasing the measured voltage from the sensor by the values determined by the sensor calibration process.

The metric used to determine the accuracy of the force resolved by the joint torque sensor is the RMS error compared to the six-axis force/torque sensor (see Figure 6). The previous section shows that the six-axis sensor is quite accurate throughout the workspace. The initial reading of the joint sensors is subtracted from values to cancel the disturbance due to the weight of the manipulator.

The dominant source of error is a disturbance torque (about the pitch axis) that generates a false reading of the torque in Joint 1 (the base yaw joint). Undesirable flexing of the

torque sensor mostly likely causes the false reading. The effect of the false torque measurement is a large error in the resolved force in the y direction. The disturbance load is caused by a combination of the weight of the manipulator and the load at the end-effector. Thus the error in the joint 1 torque grows as the end-effector location moves farther forward because the manipulator center of mass shifts forward as well. Figure 7 shows the measured joint 1 torque of the *freestanding* manipulator versus the pitch torque as measured by the joint 2 torque sensor. The expected value of the joint 1 torque sensor reading should be near zero since the joint 1 axis is approximately parallel to the gravity vector. The graph shows that the torque in joint 1 increases with the pitch torque. The applied force at the end-effector can add or subtract the pitch torque at the base of the manipulator depending on the direction of the load and location of the end-effector with respect to the base. Thus the force error in the y direction (normal to operational plane) varies as the end-effector applies a load onto the environment.

In the case where the number of torque sensors is less than six, the full contact wrench (three forces and three torques) cannot be determined. Thus, some assumptions must be made about the end-effector load. In this case the moment loads are assumed to be zero. This approximation is valid since there is one well-defined contact point in these experiments. However in a mission operation this most likely will not be the case. In a drilling operation, for example, it is likely that there will be either (1) multiple contact points (e.g. tines) or (2) moment loads from the contact interaction and an ambiguous contact point location (e.g. drilling reaction loads). This would result in the incorrect estimation of the force acting at the end-effector.

Repeatability – One element that may affect the repeatability of this sensor is the fact that these sensors are influenced by the weight of the manipulator. Thus, the value of the load applied at the end-effector must be found by either zeroing the sensors when the manipulator is close to the contact configuration before it has made contact, or by canceling the joint torque components due to the weight of the manipulator. The latter method requires knowledge of the mass center location of each of the manipulator's moving segments and the pose of manipulator with respect to gravity. Since these are not available for these experiments, the former method is used.

Another source of non-repeatability is the deviation of the sensor axis relative to the contact location due to the flexing or drooping of the manipulator. This would change the scale factor that each torque sensor reading contributes to the applied load. These deviations could be estimated using a flexible kinematics model.

The effectiveness of the joint torque sensors is highly dependent on the pose of the manipulator. Even when there are enough sensors to resolve the wrench at the end-effector, there are certain configurations where the load will be unobservable. These occur when the transpose of the Jacobian matrix becomes singular and thus is not invertible. Also, as the singularity configuration approaches, the scale between the torque measurements and certain load components become large, making these computed load components have lower signal-to-noise ratios.

Sensor Breadth – This sensing technique cannot measure the moments at the contact point, nor can it estimate the contact point location. It can detect collisions of the arm with the environment.

Link Strain Gauge Sensors

Accuracy – The measured moment load at each link is determined by scaling and biasing the measured voltage from the strain gauges by the values determined by the sensor calibration process. The expected values are calculated by taking the cross product of the vector from the gauge location to the point of contact and the measured force at the point of contact (using the wrist-mounted force sensor) (see Equation 4).

The goal is to find a method to assess the quality (in terms of accuracy) of the moments measured at the links. This information could be used to weight the sensed moments in favor of the more accurate sensor depending on the operational conditions. The most error prone situation is clearly when the force is applied in the y direction (see Figure 8 and Figure 9).

The metric used to determine the accuracy of the force resolved by the link sensor approach is the RMS error between the estimate and the six-axis force/torque sensor (see Figure 10) force values. The previous section shows that the six-axis sensor is as accurate as the load cell through out the workspace. The initial reading of the link sensors is subtracted from values to cancel the disturbance due to the weight of the manipulator.

This sensing approach is very susceptible to errors both mechanically and in the force estimation. The mechanical errors are due to ill-conditioned applied force, when the resultant force vector passes through or near a strain gauge bridge center location. Another source of error is the flexibility of the manipulator. This is especially true when the applied force is perpendicular to the plane of the manipulator (the y direction for these tests) and as the manipulator becomes more out-stretched.

Finally, the estimation of forces can exacerbate the error in the measured moments, especially when the resultant force vector passes through or near a strain gauge bridge center location. This is because the measured moment errors are amplified due to the small moment arm to the point of contact.

Repeatability – This sensing technique has the same configuration dependency as the joint torque sensors.

Sensor Breadth – This sensing technique cannot measure the moments at the contact point, nor can it estimate the contact point location. It can detect collisions of the arm with the environment.

Motor Current Sensors

Accuracy – The five current measurements are converted to joint torques using each motor's corresponding torque constant, gear ratio, and geartrain efficiency. Just as with the joint torque sensors, the truncated 5x3 Jacobian is used. The pseudo-inverse of this Jacobian is multiplied by the vector of torques to calculate the three forces at the end-effector.

These calculated forces are compared to the same three forces as measured by the ATI force torque sensor at the end-effector. The results of the three sets of experiments are plotted in Figure 11.

Repeatability – The current sensors are consistently able to produce a strong estimate of the force in the applied direction. In all three tests (X, Y, and Z) the average error in the relevant direction is less than 5 N. This accuracy is seen across the entire range of tests.

In many of the tests there is significant error in the direction where no force is being applied, in some cases as many as 15 N above the desired level of zero. This is most likely due to the same crosstalk as is seen by the joint torque sensors and could be solved in the same manner (see Impact on Flight Design section).

These sensors also have the same configuration dependency as the joint torque sensors and the link strain gauges.

Sensor Breadth – The motor current sensor is simply an indirect means of measuring torque at the joint. It therefore has the same breadth as the joint torque sensors discussed above.

A limitation of the motor current sensors is that they are only accurate when the force is being actively applied by the arm (e.g. in the experiments, after the 40 N threshold was reached and the Cartesian velocity was reversed, thus reducing the force, the motor currents became uncorrelated to the applied load). This is due to stiction effects in the geartrain and is a problem unique to this sensor.

Flexibility Modeling

Accuracy – The accuracy of this approach is a strong function of the magnitude of the force being applied. Along the direction of force application the average error for a 40 N force was approximately 5 N. For lower forces (<20 N) the average error was ~1 N and for higher forces (60 N) the average error was ~20 N. No analysis of off-axis errors was performed. A more detailed description of the results of this technique can be found in [1].

Repeatability – This sensing technique has similar configuration dependencies as the other joint and link sensing techniques.

Sensor Breadth – This sensing technique cannot measure the moments at the contact point, nor can it estimate the contact point location. It also cannot detect collisions of the arm with the environment.

Table 1: Bounds and standard deviation of the force measurement error: the 6-axis sensor reading (in the direction of the load cell) minus the load cell reading.

	Error in Force for X Test			Error in Force for Y Test			Error in Force for Z Test		
	Run #	RMS (N)	Std	Run #	RMS (N)	Std	Run #	RMS (N)	Std
Minimum	15	0.443	0.453	11	0.465	0.420	16	0.411	0.213
Maximum	1	0.728	0.716	27	0.989	0.487	2	1.187	0.783

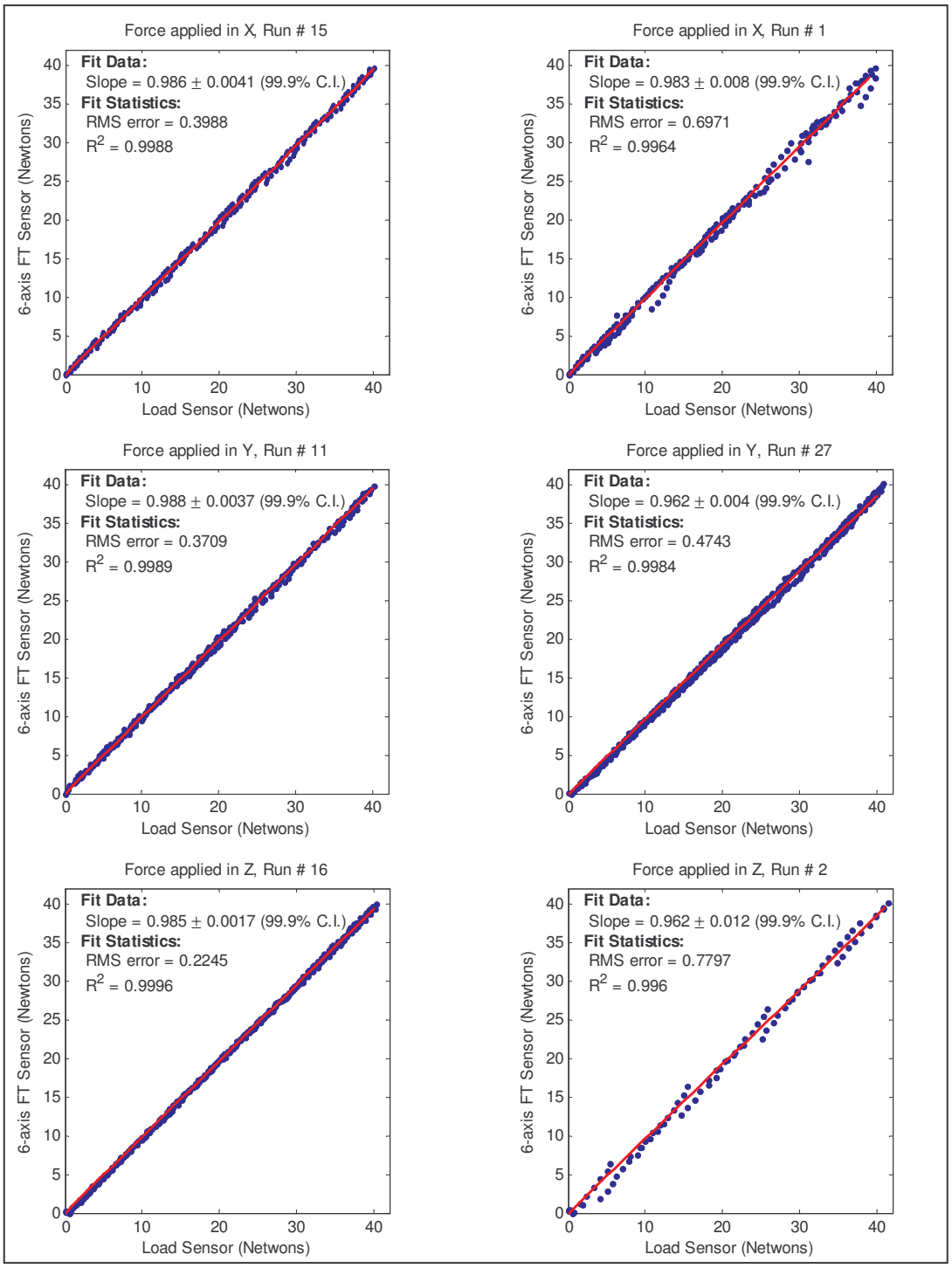

Figure 5: Least-Squares Fits of Force/Torque Sensor vs. Load Cell

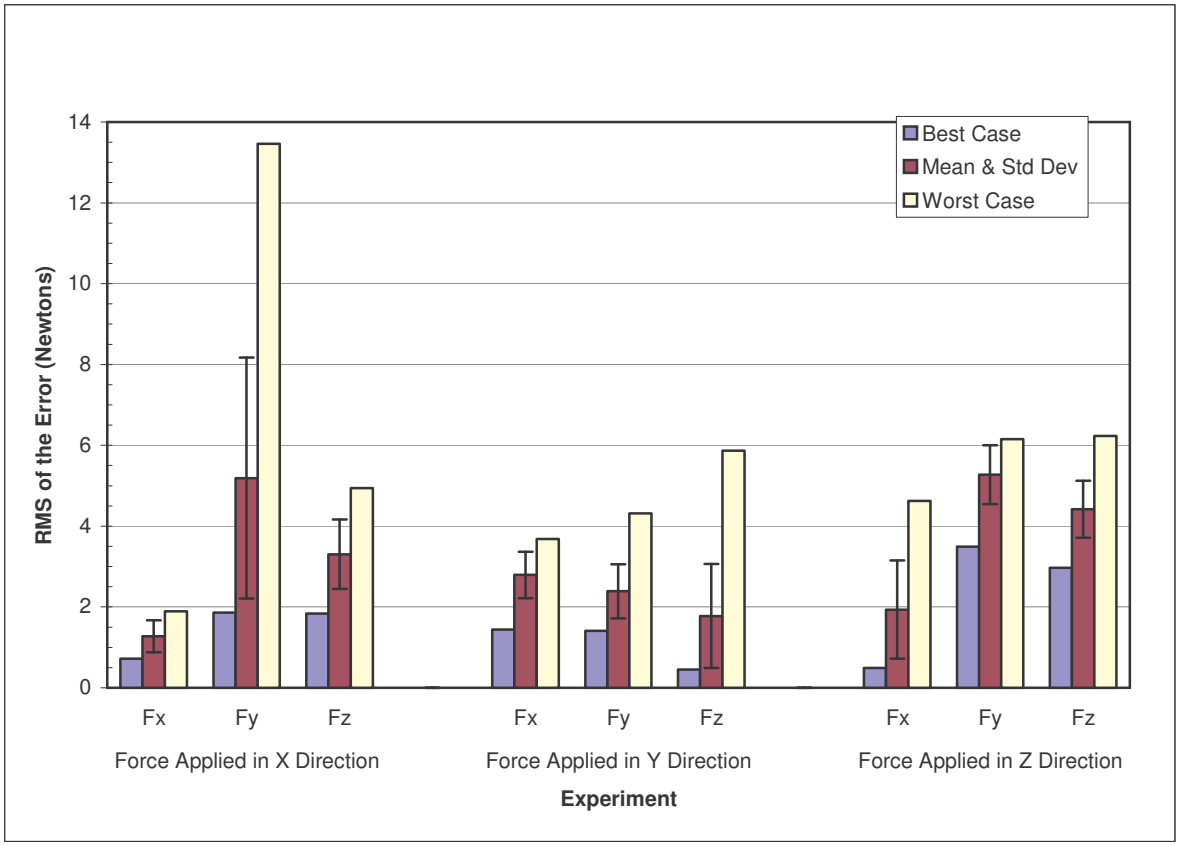

Figure 6: Joint Torque Sensor vs. Six-Axis Force/Torque Sensor

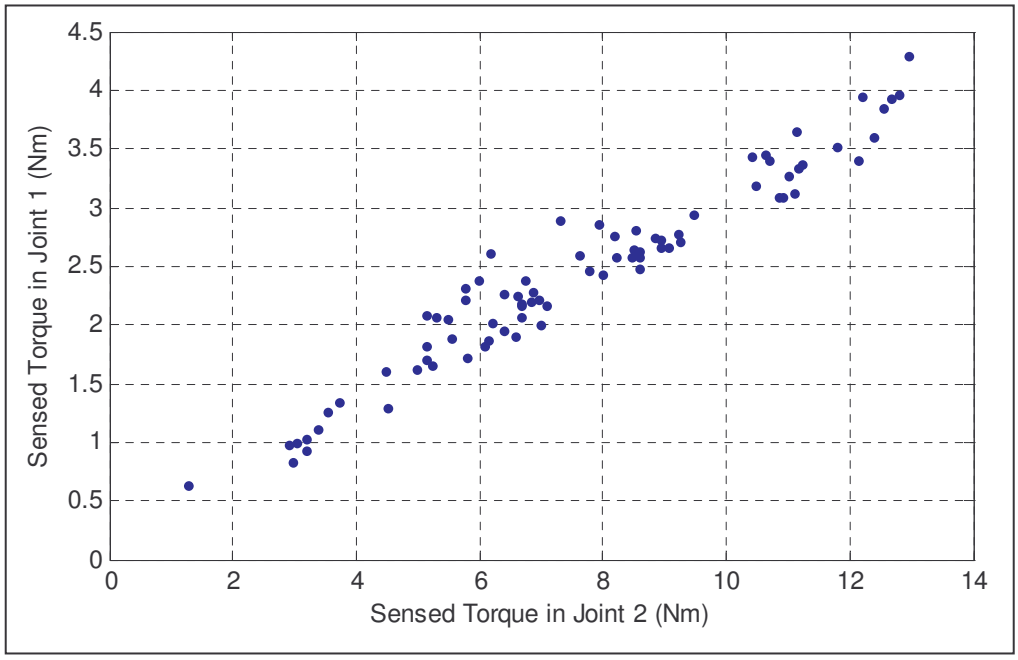

Figure 7: Joint Torque 'Crosstalk' – Measurements of Freestanding Manipulator in Various Poses

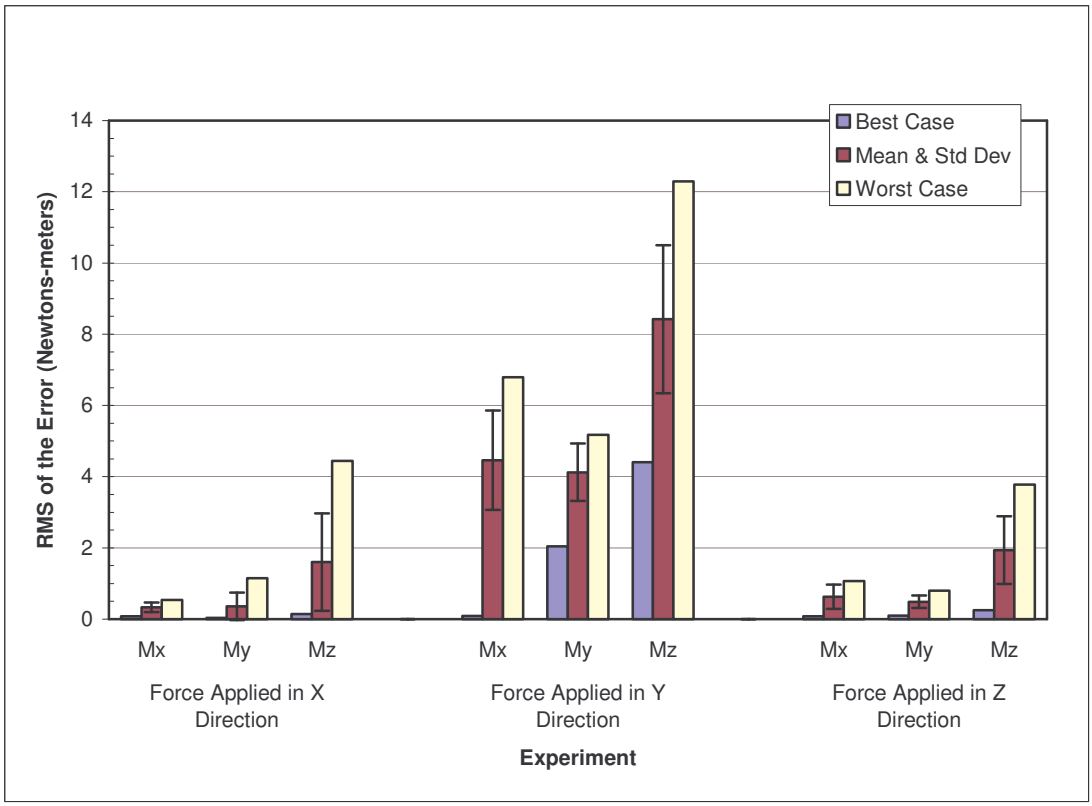

Figure 8: Link 1 Sensor Moments vs. Computed Moments

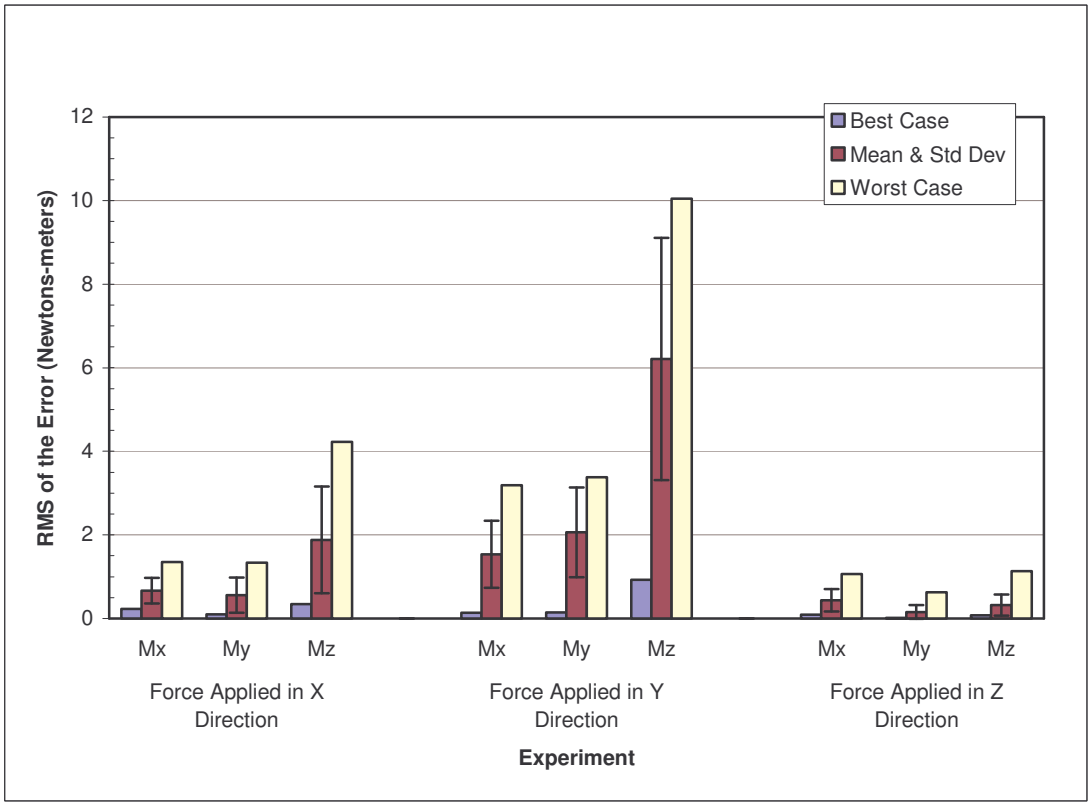

Figure 9: Link 2 Sensor Moments vs. Computed Moments

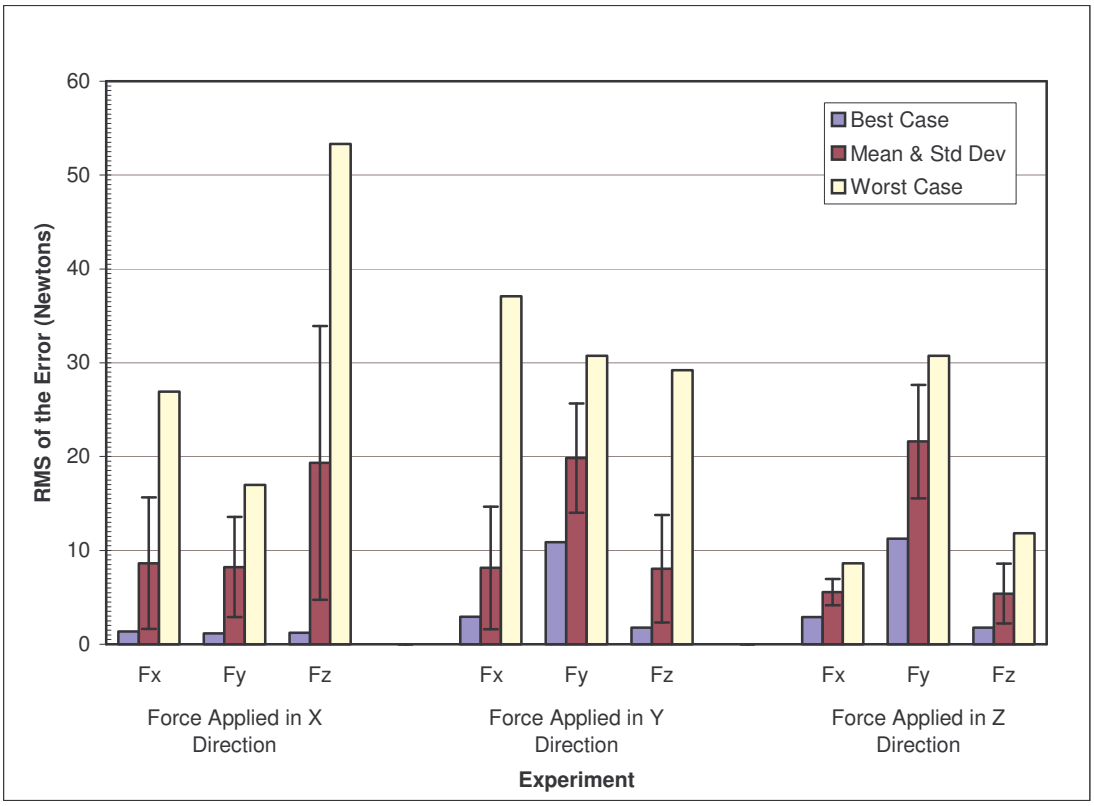

Figure 10: Link Sensors vs. Six-Axis Force/Torque Sensor

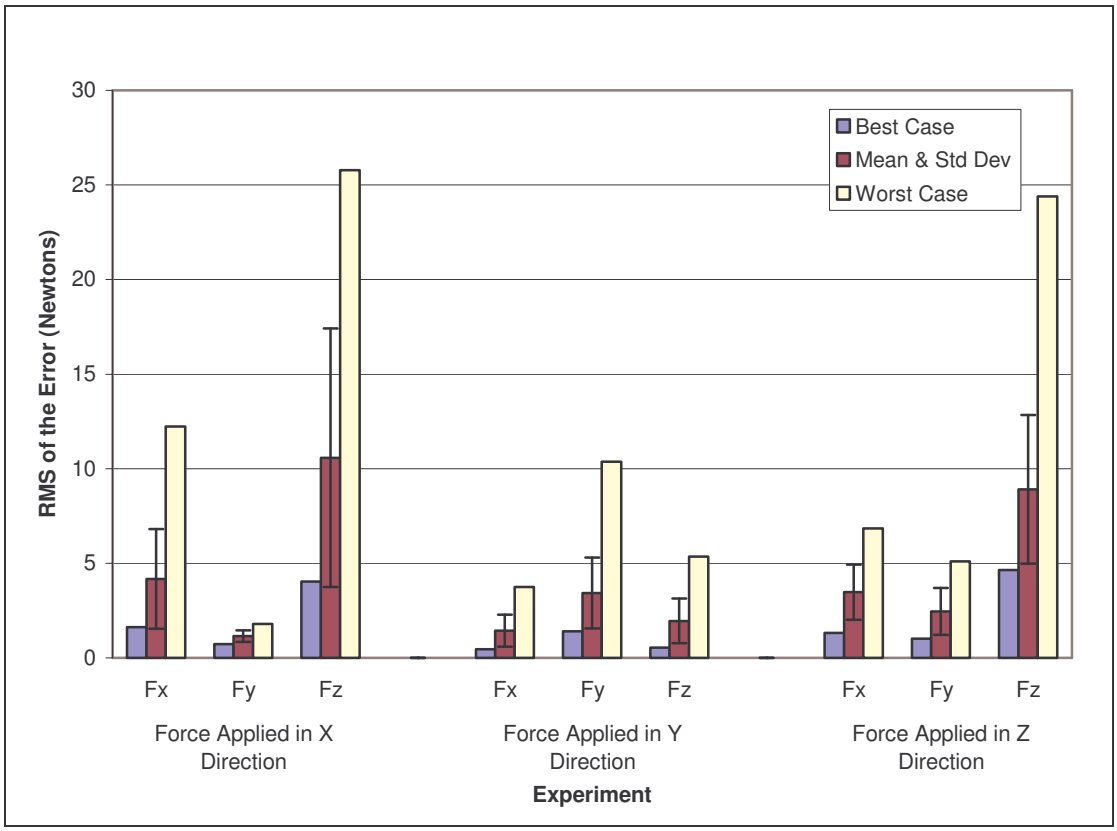

Figure 11: Current Sensor vs. Six-Axis Force Sensor

4. IMPACT ON FLIGHT DESIGN

The five sensing techniques were chosen because they span the known trade space of force sensing in terms of complexity (the flexibility model being the simplest and the six-axis force/torque sensor being the most complex). Described in this section are the impacts of the complexity on a flight design.

The six-axis force/torque sensor, the joint torque sensors, and the link strain gauge sensors all use strain gauges as the fundamental sensing element. Since a strain gauge has never been flown on a landed mission this adds a certain amount of risk to these approaches. There are currently efforts underway to qualify a low temperature single-axis load cell for the 2009 Mars Science Laboratory (MSL) mission. If this qualification effort is successful, then the risk of using any of these three techniques will be significantly reduced. The other issue that contributes to the complexity of the strain gauges is the circuitry required to condition the strain gauge signals. Wheatstone bridges, precise power supplies, and low-pass filters are all necessary to create useful signals. The location of this circuitry needs to be as close as possible to the actual strain gauges to reduce the noise on the signal making it likely that this circuitry will have to operate over extreme temperature and pressure ranges.

Six-Axis Force/Torque Sensor

In addition to the above issues regarding the strain gauges the six-axis force/torque sensor has its own unique issues. The most significant of these is the fact that six sensors are co-located. Depending on the architecture this could be a benefit or a detriment. The fact that the sensor is located at the end of the manipulator also means that all of the wiring must travel through the entire arm (unless a distributed avionics approach was taken, and a local set of avionics was available at the end of the arm).

Joint Torque Sensors

The primary challenge of integrating joint torque sensors is to design the sensor in a way that can reject off-axis disturbances. The strain gauges can be arranged in a way to improve this; however, requirements on the joint design increase significantly in order to completely isolate the single axis joint torque from any other torques. As with the six-axis force/torque sensor, wiring and signal conditioning are also issues.

Link Strain Gauge Sensors

The strain gauge issues mentioned above and similar wiring and signal conditioning issues are present with the link strain gauge sensors.

Motor Current Sensors

Because motor current sensors have flown before on a landed mission (MER) the impact on the flight design is well known and minimal.

Flexibility Modeling

The flexibility modeling has the lowest impact on flight design. The only sensing requirements it has are of joint positions, which is required for any other robotic application, so the impact is negligible.

5. CONCLUSIONS

A comprehensive set of experiments and analysis was performed to assess the relative accuracy, repeatability, breadth, and impact on flight of each of the five sensing techniques. The a summary of the results of the relative accuracy of each of the techniques are shown in Figure 12.

It is clear that, in terms of accuracy, repeatability, and configuration independence, the six-axis force/torque sensor is the best. This technique, however, is arguably the most complex of the solutions.

The two joint level techniques (the joint torque sensors and the motor current sensors) both suffer from a 'crosstalk' effect that may be solved with a more robust joint design, but it is uncertain how difficult it will be to isolate the torques sufficiently.

In a fully compensated (all axes) force controller these off-axis errors would be unacceptable and would make the control algorithm unpredictable and possibly unstable. Because the on-axis force estimates are relatively accurate a single axis force control algorithm could be devised for single axis operations such as drilling or coring, but even in these cases if any off-axis disturbance rejection is necessary, these sensors would not allow for this capability.

As can be seen in Figure 12, the link strain gages are actually less accurate than the flexible kinematics. The only reason that this sensing technique would be used over the flexible kinematics, is that it can detect arm collisions.

All three of the sensing techniques that use strain gauges (six-axis force/torque sensor, joint torque sensors, and link strain gauges) are higher risk solutions because, as of the writing of this paper, no strain gauge has ever been flown on a landed mission. An effort was described that will qualify a low temperature single-axis load cell, which uses a strain gauge. If this effort is successful, the risk associated with using these sensors will be reduced significantly.

There are many reasons to use force sensing on a manipulator. One of the most significant is that accurate force measurement can significantly reduce the design margins of the manipulator, resulting in lower mass and lower power designs. Another reason that offsets the increase in complexity associated with these approaches is the fact that contact sensors could be replaced by any of these sensing techniques. A good demonstration of this is discussed in [2].

Force sensing enables or enhances many planetary arm operations. Operations such as trenching and rock abrading can be performed more precisely than without force sensing. Operations such as coring, assembling, constructing, and grasping are enabled by force sensing, significantly increasing the capabilities of planetary manipulators.

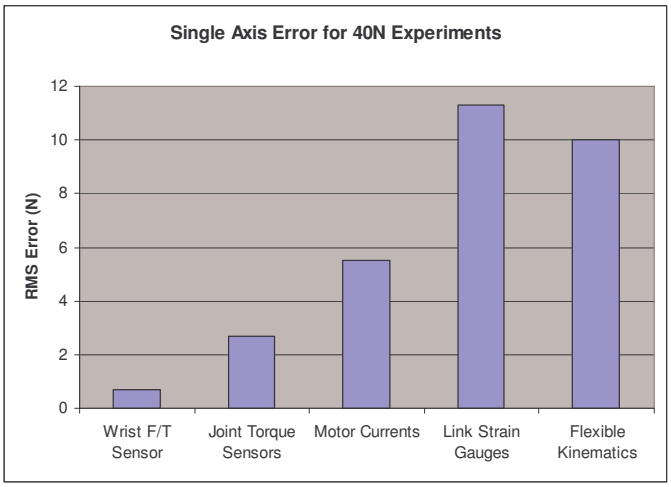

Figure 12: Comparison of the Errors of the Five Techniques

5. AKNOWLEDGEMENT

The research described in this publication was carried out at the Jet Propulsion Laboratory, California Institute of Technology under contract from the National Aeronautics and Space Administration (NASA), with funding from the Mars Technology Program, NASA Science Mission Directorate.

REFERENCES

[1] Eric T. Baumgartner, Robert G. Bonitz, Joseph P. Melko, Lori R. Shiraishi and P. Chris Leger, "The Mars Exploration Rover Instrument Positioning System," *Proceedings of the IEEE Aerospace Conference*, March 2005.

[2] Antonio Diaz-Calderon and Paul Backes, "Automated Sampling Acquisition on Planetary Surfaces," *JPL Internal Document,* November, 2005.

BIOGRAPHY

Daniel Helmick *received his B.S degree in Mechanical Engineering from Virginia Polytechnic Institute and State University and his M.S. in Mechanical Engineering with a specialization in controls from Georgia Institute of Technology in 1996 and 1999 respectively. Since June 1999 he has been working at the Jet Propulsion Laboratory on robotics research projects involving vision/sensor based control of robots, state estimation, manipulation, and navigation and mobility algorithms. He has worked on robotic vehicles covering a wide range of functionality, including: Mars research rovers for rough terrain mobility; small, tracked robots for urban mobility; a cryobot for ice penetration; and reconfigurable wheeled robots for Mars exploration. His research interests include: sensor-based control of robots, sensor fusion and state estimation, and rover navigation and mobility.*

Avi Okon *has been at NASA's Jet Propulsion Laboratory since 2001. He has received his Bachelors of Science and Master of Science degree in Mechanical Engineering from the University of California at Los Angeles. Some of his responsibilities at JPL include the development of hardware and feedback control algorithms for limbed and cooperative robotic systems used for construction. His research interests include: motion and force control, control of multi-agent robots, and robot design.*

Matthew DiCicco *is an associate member of technical staff at the NASA Jet Propulsion Laboratory in Pasadena, CA. He recieved an MS from MIT in 2005 where he studied manipulator control in the Field and Space Robotics Laboratory. He recieved a BS in mechanical engineering from Carnegie Mellon in 2003. At JPL he has continued his work on robot manipulators through research and development tasks and flight projects as a member of the Mobility and Manipulation Group.*

Appendix A

Table 2: End-Effector Test Positions (in manipulator base frame)

Forces applied in X direction						Forces applied in Y direction						Forces applied in Z direction					
Run	Contact Pose (mm, deg)					Run	Contact Pose (mm, deg)					Run	Contact Pose (mm, deg)				
	x	y	z	az	el		x	y	z	az	el		x	y	z	az	el
1	593	-23	369	-180	0	1	195	36	254	-178	0	1	161	-23	108	-180	1
2	596	-23	268	-180	1	2	199	38	204	-178	0	2	154	-23	210	-180	1
3	602	-23	166	-180	1	3	202	40	154	-178	0	3	150	-23	291	-180	1
4	504	-23	164	-180	1	4	193	41	305	-178	1	4	245	-23	294	-180	0
5	500	-23	266	-180	1	5	191	43	356	-178	1	5	249	-23	209	-180	0
6	493	-23	363	-180	0	6	188	44	406	-178	1	6	255	-23	107	-180	0
7	390	-23	411	-180	0	7	240	45	408	-178	1	7	354	-23	112	-180	0
8	396	-23	312	-180	1	8	242	47	357	-178	1	8	349	-23	214	-180	0
9	402	-23	212	-180	1	9	244	49	307	-178	1	9	344	-23	296	-180	0
10	408	-23	111	-180	1	10	247	50	257	-178	1	10	444	-23	297	-180	0
11	307	-23	103	-180	0	11	250	51	207	-178	1	11	448	-23	217	-180	0
12	302	-23	206	-180	0	12	252	53	157	-178	1	12	453	-23	117	-180	0
13	297	-23	307	-180	0	13	304	55	159	-178	1	13	552	-23	122	-180	0
14	293	-23	408	-180	1	14	302	56	207	-178	1	14	549	-23	220	-180	0
15	190	-23	404	-180	0	15	299	58	257	-178	1	15	544	-23	292	-180	0
16	196	-23	305	-180	0	16	297	59	308	-178	1	16	558	-23	19	-180	0
17	203	-23	205	-180	0	17	294	61	359	-178	1	17	459	-23	15	-180	0
18	211	-23	104	-180	0	18	291	62	409	-178	2	18	359	-23	11	-180	0
						19	340	63	411	-178	2	19	260	-23	7	-180	0
						20	342	66	361	-179	2	20	160	-23	4	-180	0
						21	345	68	312	-179	2	21	626	-23	27	-180	0
						22	346	70	263	-179	2	22	621	-23	120	-180	1
						23	353	71	209	-179	2	23	616	-23	222	-180	1
						24	355	73	159	-179	2	24	612	-23	293	-180	1
						25	404	74	161	-179	2						
						26	401	74	212	-179	2						
						27	398	75	263	-179	3						
						28	395	75	314	-179	3						
						29	392	76	365	-179	3						
						30	390	77	405	-179	3						
						31	487	78	410	-179	3						
						32	495	80	316	-180	4						
						33	499	83	217	-180	4						
						34	503	84	118	-180	4						
						35	607	88	118	-180	0						
						36	602	89	221	-180	1						
						37	595	90	323	-180	1						
						38	584	34	384	-180	0						